J|A|C|S ARTICLES

Published on Web 04/20/2010

Probing the Structural Evolution of Medium-Sized Gold Clusters: Au_n^- ($n = 27-35$)

Nan Shao,[†] Wei Huang,[‡] Yi Gao,[†] Lei-Ming Wang,[‡,§] Xi Li,[‡,||] Lai-Sheng Wang,*[,‡] and Xiao Cheng Zeng*[,†]

Department of Chemistry and Nebraska Center for Materials and Nanoscience, University of Nebraska—Lincoln, Lincoln, Nebraska 68588, and Department of Chemistry, Brown University, Providence, Rhode Island 02912

Received March 13, 2010; E-mail: lai-sheng_wang@brown.edu; xczeng@phase2.unl.edu

Abstract: The structural evolution of negatively charged gold clusters (Au_n^-) in the medium size range for $n = 27-35$ has been investigated using photoelectron spectroscopy (PES) and theoretical calculations. New PES data are obtained using Ar-seeded He supersonic beams to achieve better cluster cooling, resulting in well-resolved spectra and revealing the presence of low-lying isomers in a number of systems. Density-functional theory calculations are used for global minimum searches. For each cluster anion, more than 200 low-lying isomers are generated using the basin-hopping global minimum search algorithm. The most viable structures and low-lying isomers are obtained using both the relative energies and comparisons between the simulated spectra and experimental PES data. The global minimum structures of Au_n^- ($n =$ 27, 28, 30, and 32−35) are found to exhibit low-symmetry core−shell structures with the number of core atoms increasing with cluster size: Au_{27}^-, Au_{28}^-, and Au_{30}^- possess a one-atom core; Au_{32}^- features a three-atom triangular core; and Au_{33}^- to Au_{35}^- all contain a four-atom tetrahedral core. The global searches reveal that the tetrahedral core is a popular motif for low-lying structures of Au_{33}^- to Au_{35}^-. The structural information forms the basis for future chemisorption studies to unravel the catalytic effects of gold nanoparticles.

Gold nanoparticles and clusters possess interesting physical and chemical properties that can be exploited for applications in catalysis and biology.[1] These novel properties result from the strong relativistic effects of gold,[2] which result in significant s−d hybridization relative to that of other coinage metals. In particular, the relativistic effects have led to unusual structures in gold nanoclusters. For example, gold cluster anions (Au_n^-) display remarkable planar (2D) structures up to $n = 12$.[3,4] Beyond $n = 12$, even more exotic structures are possible, such as the golden pyramid[5,6] and hollow golden cages.[7] A number of experimental techniques have been used to provide structural information for gold clusters, such as ion mobility,[3a] photoelectron spectroscopy (PES),[4a,5,6e,7] trapped ion electron diffraction (TIED),[6f,8a,c] and infrared vibrational spectroscopy.[6g] To date, atomic structures of gold anion clusters in the size range of $n = 3-20$ have been relatively well established.[3−9] The 2D to 3D structural transition occurs at Au_{12}^-, for which both the 2D cluster and a 3D shell-like structure coexist.[4b,c] Clusters in the size range of Au_{13}^- to Au_{15}^- possess flat cage (or shell-

[†] University of Nebraska—Lincoln.
[‡] Brown University.
[§] Current address: Department of Physics, University of Pittsburgh, Pittsburgh, Pennsylvania 15260.
[||] Current address: Department of Environmental Science & Engineering, Fudan University, Shanghai 200433, PR China.

(1) (a) Haruta, M. *Catal. Today* **1997**, *36*, 153. (b) Chen, M. S.; Goodman, D. W. *Science* **2004**, *306*, 252. (c) Turner, M; Golvoko, V. B.; Vaughan, O. P. H.; Abdulkin, P.; Berenguer-Murcia, A.; Tikhov, M. S.; Johnson, B. F. G.; Lambert, R. M. *Nature* **2008**, *454*, 981. (d) Herzing, A. A.; Kiely, C. J.; Carley, A. F.; Landon, P.; Hutchings, G. J. *Science* **2008**, *321*, 1331. (e) Whetten, R. L.; Khoury, J. T.; Alvarez, M. M.; Murthy, S.; Vez-mar, I.; Wang, Z. L.; Stephens, P. W.; Cleveland, C. L; Ludedtke, W. D.; Landman, U. *Adv. Mater.* **1996**, *5*, 8. (f) Mirkin, C. A.; Letsinger, R. L.; Mucic, R. C.; Storhoff, J. *Nature (London).* **1996**, *382*, 607. (g) Alivisatos, A. P.; Johnsson, K. P.; Peng, X.; Wilson, T. E.; Loweth, C. J.; Bruchez, M. P.; Schultz, P. G. *Nature (London.)* **1996**, *382*, 609. (h) Schwerdtfeger, P. *Angew. Chem., Int. Ed.* **2003**, *42*, 1892.

(2) (a) Pyykkö, P. *Chem. Rev.* **1988**, *88*, 563. (b) Pyykkö, P. *Angew. Chem., Int. Ed.* **2004**, *43*, 4412. (c) Scherbaum, F.; Grohmann, A.; Huber, B.; Krüger, C.; Schmidbaur, H. *Angew. Chem., Int. Ed.* **1988**, *27*, 1544.

(3) (a) Furche, F.; Ahlrichs, R.; Weis, P.; Jacob, C.; Gilb, S; Bierweller, T.; Kappes, M. M. *J. Chem. Phys.* **2002**, *117*, 6982. (b) Häkkinen, H.; Moseler, M.; Landman, U. *Phys. Rev. Lett.* **2002**, *89*, 033401.

(4) (a) Häkkinen, H.; Yoon, B.; Landman, U.; Li, X.; Zhai, H. J.; Wang, L. S. *J. Phys. Chem. A* **2003**, *107*, 6168. (b) Johansson, M. P.; Lechtken, A.; Schooss, D.; Kappes, M. M.; Furche, F. *Phys. Rev. A* **2008**, *77*, 053202. (c) Huang, W.; Wang, L. S. *Phys. Rev. Lett.* **2009**, *102*, 153401. (d) Ferrighi, L.; Hammer, B.; Madsen, G. K. H. *J. Am. Chem. Soc.* **2009**, *131*, 10605. (e) Mantina, M.; Valero, R.; Truhlar, D. G. *J. Chem. Phys.* **2009**, *131*, 064706. (f) Xiao, L.; Wang, L. *Chem. Phys. Lett.* **2004**, *392*, 452.

(5) Li, J.; Li, X.; Zhai, H. J.; Wang, L. S. *Science* **2003**, *299*, 864.

(6) (a) Fernandez, E. M.; Soler, J. M.; Garzon, I. L.; Balbas, L. C. *Phys. Rev. B* **2004**, *70*, 165403. (b) King, R. B.; Chen, Z.; von Ragué Schleyer, P. *Inorg. Chem.* **2004**, *43*, 4564. (c) Apra, E.; Ferrando, R.; Fortunelli, A. *Phys. Rev. B* **2006**, *73*, 205414. (d) Kryachko, E. S.; Remacle, F. *Int. J. Quantum Chem.* **2007**, *107*, 2922. (e) Yoon, B.; Koskinen, P.; Huber, B.; Kostko, B.; Issendorff, B. v.; H kkinen, H; Moseler, M.; Landman, U. *ChemPhysChem* **2007**, *8*, 157. (f) Lechtken, A.; Neiss, C.; Stairs, J.; Schooss, D. *J. Chem. Phys.* **2008**, *129*, 154304. (g) Gruene, P.; Rayner, D. M.; Redlich, B.; van der Meer, A. F. G.; Lyon, J. T.; Meijer, G.; Fielicke, A. *Science* **2008**, *321*, 674. (h) Zubarev, D. Y.; Boldyrev, A. I. *J. Phys. Chem. A* **2009**, *113*, 866.

(7) Bulusu, S.; Li, X.; Wang, L. S.; Zeng, X. C. *Proc. Natl. Acad. Sci. U.S.A.* **2006**, *103*, 8326.

 10.1021/ja102145g

like) structures. Au_{16}^- and Au_{17}^- are shown to possess hollow cage structures,[7,8] and Au_{19}^- and Au_{20}^- have distinct tetrahedral structures.[5,6] The cage-to-pyramidal structure transition has been established recently to occur at Au_{18}^-, for which both the cage and pyramidal isomers coexist.[8b]

Beyond Au_{20}^-, only a few structural studies have been carried out experimentally.[10−13] In a joint PES and DFT study for $n = 21-25$, Bulusu et al. showed that other low-symmetry structures were competitive with the pyramid-based structures in the size range of $n = 21-23$.[10b] Au_{24}^- was suggested to be a low-symmetry tubular structure, which is different from the higher-symmetry tubular-type structures reported previously[8a] by a TIED experiment and DFT studies. Au_{25}^- was found to be the first cluster to exhibit a core−shell structure with a single-atom core and 24-atom shell. Although neutral Au_{32} was reported to possess an icosahedral cage structure,[14] a combined DFT and PES study showed that the Au_{32}^- cluster anion possesses a more compact core−shell-type structure.[12a] Subsequent theoretical calculations support this conclusion.[12b,c] The structures of the Au_{34}^- cluster have been studied both by TIED and PES,[13a,c] showing that its global minimum also consists of core−shell-type structures with a four-atom core. A combined PES and theoretical study showed that Au_{55}^- is not icosahedral,[10a] different from I_h Cu_{55}^- and Ag_{55}^-, in agreement with previous theoretical predictions that Au_{55} is amorphous.[15] The amorphous Au_{55} cluster was understood subsequently on the basis of the relativistic contraction of the surface layer by analogy to bulk gold surfaces by Huang et al. in a combined PES and DFT study.[16] In the same study, Huang et al. also reported the structures of the largest size-selected Au_n^- clusters that have been characterized experimentally thus far. They found that the Au_{58}^- cluster possesses a very stable, spherical core−shell structure. Larger clusters from Au_{59}^- to Au_{64}^- are formed simply by attaching the extra atoms to the surface of Au_{58}^- with minor structural distortions.

Structural determination for larger gold clusters becomes increasingly more challenging, and global minimum searches are essential because of the sheer number of possible atomic arrangements. Except for Au_{32}^- and Au_{34}^-,[12,13] DFT-based global searches have not been done for gold clusters in the range of Au_{26}^- to Au_{35}^-. In fact, the global minima of Au_{32}^- and Au_{34}^- are still controversial. Ji et al.[12a] first reported that Au_{32}^- is a core−shell cluster with a three-atom triangular core. Further first-principals calculations suggested that the global minimum of Au_{32}^- contains a four-atom tetrahedral core.[12b,c] For Au_{34}^-, the combined TIED and DFT study resulted in a C_3 core−shell cluster with a four-atom tetrahedral core,[13a,b] but the PES and DFT study found two low symmetry (C_1) core−shell structures, both with a four-atom tetrahedral core, competing for the global minimum.[13c] The low-symmetry C_1 structure for Au_{34}^- has been confirmed by two subsequent DFT studies.[13d,e]

The aim of the current study is to explore the systematic structural evolution of negatively charged gold clusters in the size range of $n = 27-35$. We conducted new PES experiments using Ar-seeded He supersonic beams to achieve better cluster cooling, yielding well-resolved spectra and isomer information in a number of cases. In conjunction with DFT-based global minimum searches, we have identified the most stable structures and low-lying isomers for Au_n^- ($n = 27$, 28, 30, and 32−35). The obtained structures reveal generic structural motifs and structural trends for gold clusters in this size range, which will be valuable for future studies of their catalytic properties (e.g., CO oxdidation[17]).

Experimental and Theoretical Methods

Photoelectron Spectroscopy. The PES experiment was performed using a magnetic-bottle apparatus equipped with a laser vaporization supersonic cluster source and a time-of-flight mass analyzer.[18] A pulsed laser beam was focused onto a pure gold disk target, generating a plasma containing gold atoms. A high-pressure helium carrier gas pulse was delivered to the nozzle simultaneously, cooling the plasma and initiating nucleation. As shown previously,[19] by carefully controlling the resident time of the clusters in the nozzle, relatively cold clusters can be produced from our laser vaporization supersonic cluster source. The cooling effects have been confirmed recently by the observation of van der Waals complexes of gold cluster anions with Ar or O_2.[4c,8b,20] In the present study, relatively cold Au_n^- clusters were produced using a helium carrier gas seeded with 5% Ar. Clusters of interest were selected by a mass gate and decelerated before being photodetached by a 193 nm laser beam from an ArF excimer laser. Photoelectrons were collected with a magnetic bottle at nearly 100% efficiency in a 3.5-m-long electron flight tube for kinetic energy analyses. The photoelectron kinetic energies were calibrated by the known spectra of Au^- and subtracted from the photon energies to obtain the

(8) (a) Xing, X; Yoon, B; Landman, U; Parks, J. H. *Phys. Rev. B* **2006**, *74*, 165423. (b) Huang, W; Bulusu, S; Pal, R; Zeng, X. C.; Wang, L. S. *ACS Nano* **2009**, *3*, 1225. (c) Lechtken, A.; Neiss, C.; Kappes, M. M.; Schooss, D. *Phys. Chem. Chem. Phys.* **2009**, *11*, 4344. (d) Bulusu, S.; Zeng, X. C. *J. Chem. Phys.* **2006**, *125*, 154303.

(9) (a) Huang, W.; Pal, R.; Wang, L. M.; Zeng, X. C.; Wang, L. S. *J. Chem. Phys.* **2010**, *132*, 054305. (b) Wang, L. M.; Pal, R.; Huang, W.; Li, X.; Zeng, X. C.; Wang, L. S. *J. Chem. Phys.* **2010**, *132*, 114306.

(10) (a) Häkkinen, H.; Moseler, M.; Kostko, O.; Morgner, N.; Hoffmann, M. A.; von Issendorff, B. *Phys. Rev. Lett.* **2004**, *93*, 093401. (b) Bulusu, S.; Li, X.; Wang, L. S.; Zeng, X. C. *J. Phys. Chem. C* **2007**, *111*, 4190.

(11) Taylor, K. J.; Pettiette-Hall, C. L.; Cheshnovsky, O.; Smalley, R. E. *J. Chem. Phys.* **1992**, *96*, 3319.

(12) (a) Ji, M.; Gu, X.; Li, X.; Gong, X. G.; Li, J.; Wang, L. S. *Angew. Chem., Int. Ed.* **2005**, *44*, 7119. (b) Jalbout, A. F.; Contreras-Torres, F. F.; Përez, L. A.; Garzón, I. L. *J. Phys. Chem. A* **2008**, *112*, 353. (c) Johansson, M. P.; Vaara, J.; Sundholm, D. *J. Phys. Chem. C* **2008**, *112*, 19311.

(13) (a) Lechtken, A.; Schooss, D.; Stairs, J. R.; Blom, M. N.; Furche, F.; Morgner, N.; Kostko, O.; von Issendorff, B.; Kappes, M. M. *Angew. Chem., Int. Ed.* **2007**, *46*, 2944. (b) Doye, J. P. K.; Wales, D. J. *New J. Chem.* **1998**, *22*, 733. (c) Gu, X.; Bulusu, S.; Li, X.; Zeng, X. C.; Li, J.; Gong, X. G.; Wang, L. S. *J. Phys. Chem. C* **2007**, *111*, 8228. (d) Santizo, I. E.; Hidalgo, F.; Perez, L. A.; Noguez, C.; Garzón, I. L. *J. Phys. Chem. C* **2008**, *112*, 17533. (e) Vargas, A.; Santarossa, G.; Inannuzzi, M.; Baiker, A. *Phys. Rev. B* **2009**, *80*, 195421.

(14) (a) Johansson, M. P.; Sundholm, D.; Vaara, J. *Angew. Chem., Int. Ed.* **2004**, *43*, 2678. (b) Gu, X.; Ji, M.; Wei, S. H.; Gong, X. G. *Phys. Rev. B* **2004**, *70*, 205401.

(15) (a) Garzón, I. L.; Michaelian, K.; Beltrán, M. R.; Posada-Amarillas, A.; Ordejón, P.; Artacho, E.; Sánchez-Portal, D.; Soler, J. M. *Phys. Rev. Lett.* **1998**, *81*, 1600. (b) Michaelian, K.; Rendon, N.; Garzon, I. L. *Phys. Rev. B* **1999**, *60*, 2000. (c) Darby, S.; Mortimer-Jones, T. V.; Johnston, R. L.; Roberts, C. *J. Chem. Phys.* **2002**, *116*, 1536. (d) Li, T. X.; Lee, S. M.; Han, S. J.; Wang, G. H. *Phys. Lett. A* **2002**, *300*, 86.

(16) Huang, W.; Ji, M.; Dong, C. D.; Gu, X.; Wang, L. M.; Gong, X. G.; Wang, L. S. *ACS Nano* **2008**, *2*, 897.

(17) (a) Huang, W.; Bulusu, S.; Pal, R.; Zeng, X. C.; Wang, L. S. *J. Chem. Phys.* **2009**, *131*, 234305. (b) Gao, Y.; Shao, N.; Pei, Y.; Zeng, X. C. *Nano Lett.* **2010**, *10*, 1055.

(18) Wang, L. S.; Cheng, H. S.; Fan, J. W. *J. Chem. Phys.* **1995**, *102*, 9480.

(19) (a) Akola, J.; Manninen, M.; Hakkinen, H.; Landman, U.; Li, X.; Wang, L. S. *Phys. Rev. B* **1999**, *60*, R11297. (b) Wang, L. S.; Li, X. Temperature Effects in Anion Photoelectron Spectroscopy of Metal Clusters. In *Clusters and Nanostructure Interfaces*; Jena, P., Khanna, S. N., Rao, B. K., Eds.; World Scientific: River Edge, NJ, 2000; pp 293−300.

(20) Huang, W.; Wang, L. S. *Phys. Chem. Chem. Phys.* **2009**, *11*, 2663.

reported electron binding energy spectra. For the current study, PES spectra were measured at 193 nm (6.424 eV), calibrated with the known spectrum of Au^-. The electron energy resolution was $\Delta E/E \approx 2.5\%$ (i.e., 25 meV for 1 eV electrons).

Theoretical Methods. Global minimum searches for low-lying structures of gold anion clusters Au_n^- in the size range of $n = 27-35$ was performed using the basin-hopping (BH)[21] global search method combined with DFT geometric optimization. The gradient-corrected Perdew−Burke−Ernzerhof (PBE) exchange-correlation functional[22] and the double-numerical polarized (DNP) basis set with effective core potentials (ECPs), implemented in the DMol3 4.0 software,[23] were employed for the geometric optimization. To generate isomer populations in the initial BH searches, a medium-level convergence criterion was chosen such that the optimization gradient convergence was less than 4×10^{-3} hartree/Å and the optimization energy convergence was 2×10^{-5} hartree in the DFT calculations. When more than 200 distinct isomer structures were collected, they were reoptimized at a higher level of convergence (the fine level in DMol^3): less than 2×10^{-3} hartree/Å for the gradient convergence and 1×10^{-5} hartree for the energy convergence. The isomers were ranked according to their relative energies at the higher level (the fine level in DMol^3) of optimization. Next, the top ranked 10−30 isomers were further optimized at the PBE/TZP(ZORA) level of theory, followed by photoelectron spectrum calculations, using the ADF2008 software package[24] in which a larger basis set, namely, the triple-ζ 1 polarization function (TZP) with a relativistic Hamiltonian under the zeroth-order regular approximation (ZORA), was used (Supporting Information Table S1).

In previous studies,[17a,8d] we examined several functionals (PBE, BLYP, B3LYP, LDA, BP3, TPSS, PBE0, and M06-L) to compute the electronic density of states (treated as a simulated photoelectron spectrum) of Au_{16}^- and Au_{19}^-. The PBE, PBE0, and TPSS functionals yielded good agreement with the measured spectrum for Au_{19}^-, and hybrid functionals PBE0 and B3LYP yielded good agreement with the measured spectrum for Au_{16}^-.[7] Recently, we found that it is important to include the spin−orbit (SO) effects in the calculation of the density of states in order to achieve nearly quantitative agreement between theoretical and experimental PES spectra.[17a] Here, we computed simulated spectra of all candidate isomers at the PBE0/CRENBL/SO level using the NWCHEM 5.1.1 software package,[25,26] for which the computed binding energies were based on the optimized structures at the PBE/TZP(ZORA) level of theory. Computed electronic energies of leading candidate isomers are shown in Table S2.

Comparison of Computed Spectra with the Experimental PES Data. We used three criteria in comparing the theoretical results with the experimental data to screen candidate structures: (1) the relative electronic energies, (2) the energy gap between the first and second major PES peaks (which is the HOMO−LUMO gap for neutral gold clusters with even numbers of atoms), and (3) the number of distinct peaks of simulated photoelectron spectra in the low-binding-energy range of $\lesssim$5.5 eV (primarily the gold 6s band region) and their relative positions. The first criterion addresses typical errors in DFT calculations, which are on the order of several tenths of an electronvolt in relative energies for gold clusters.[4d,e,17,27] In the present study, we used a cutoff energy of 0.4 eV at the PBE/DNP (fine) level to collect low-lying isomers. This screening step typically reduced the total number of isomers from more than 200 to 50−100.

Next, for those low-lying isomers with an energy gap within ±0.03 eV from the measured value, that is, the gap between the first and second vertical detachment energies (VDEs), their full PES spectra were computed. This screening step reduced the total number of candidate isomers from 50−100 to 10−30. The simulated spectra were then compared to the measured PES spectra to identify top candidates for the global minimum and low-lying isomers. Well-resolved PES spectra are a prerequisite for allowing meaningful comparisons with the simulated spectra. We paid particular attention to the number of peaks below 5.5 eV (usually the 6s band region with discrete peaks), the spacings among these peaks, and, to a much lesser extent, the number of peaks beyond 5.5 eV (the 5d region with more congested features). Only those isomers that meet all three criteria are considered to be top candidates for the global minimum, and their structures and computed PESs (including SO effects) are presented. In addition, structures reported in the literature are recalculated and also presented for comparison.

Results

We have measured the photoelectron spectra of Au_n^- ($n = 27-35$) at two photon energies: 266 nm (4.661 eV) and 193 nm (6.424 eV). Because of the high electron binding energies of these clusters, the 266 nm data can allow only the first few PES peaks to be observed with enhanced resolution, as shown in Figure S1. The 193 nm spectra reveal transitions both in the 6s and 5d band regions, as shown in Figure S2 and Figures 1−7. We have measured the 193 nm data under two conditions: (1) with a pure He carrier gas and (2) with a 5% Ar-seeded He carrier gas for better cluster cooling. For Au_{27}^- to Au_{33}^-, we have observed differences in the PES spectra using the Ar-seeded He carrier gas relative to data taken with the pure He carrier gas, as shown in Figures 1−5. The spectra taken with the Ar-seeded He carrier gas are slightly better resolved. The PES spectra of Au_{29}^- and Au_{31}^- were quite congested even in the low-binding-energy region (Figures S1 and S2), making it difficult to compare with simulated spectra. Therefore, these two clusters are omitted in our computational study.

The relative energies, structures, and simulated spectra for the low-lying isomers (labeled as I, II, etc.) are compared with the experimental data in Figures 1−7. For the convenience of comparison, the well-resolved low-binding-energy features in the experimental data are labeled with letters X, A, B, and so forth. The VDEs for the first (X) and second PES bands and their differences are given in Table 1.

Discussion

Au_{27}^-. The 193 nm PES spectra of Au_{27}^- obtained under the pure He carrier gas and Ar-seeded He carrier gas are shown in Figure 1a,b, respectively. Seven distinct peaks are resolved and labeled as X and A−F in the low-binding-energy range. Indeed, differences between the spectra in Figure 1a,b can be readily seen. All features are slightly better resolved in Figure 1b as a

(21) (a) Wales, D. J.; Scheraga, H. A. *Science* **1999**, *285*, 1368. (b) Yoo, S.; Zeng, X. C. *J. Chem. Phys.* **2003**, *119*, 1442. (c) Yoo, S.; Zeng, X. C. *Angew. Chem., Int. Ed.* **2005**, *44*, 1491.
(22) Perdew, J. P.; Burke, K.; Ernzerhof, M. *Phys. Rev. Lett.* **1996**, *77*, 3865.
(23) (a) Delley, B. *J. Chem. Phys.* **1990**, *92*, 508. (b) Delley, B. *J. Chem. Phys.* **2003**, *113*, 7756. DMol^3 is available from Accelrys.
(24) ADF 2008.01; SCM, Theoretical Chemistry, Vrije Universiteit, Amsterdam, The Netherlands (http://www.scm.com).
(25) Kendall, R. A.; Apra, E.; Bernholdt, D. E.; Bylaska, E. J.; Dupuis, M.; Fann, G. I.; Harrison, R. J.; Ju, J.; Nichols, J. A.; Nieplocha, J.; Straatsma, T. P.; Windus, T. L.; Wong, A. T. *Comput. Phys. Commun.* **2000**, *128*, 260.
(26) Bylaska, E. J.; et al. *NWCHEM, a Computational Chemistry Package for Parallel Computers*, version 5.1.1; Pacific Northwest National Laboratory: Richland, WA.
(27) (a) Han, Y. K. *J. Chem. Phys.* **2006**, *124*, 024316. (b) Diefenbach, M.; Kim, S. *J. Phys. Chem. B* **2006**, *110*, 21639. (c) Olson, R. M.; Varganov, S.; Gordon, M. S.; Metiu, H.; Chretien, S.; Piecuch, P.; Kowalski, K.; Kucharski, S. A.; Musial, M. *J. Am. Chem. Soc.* **2005**, *127*, 1049.
(28) (a) Fa, W.; Luo, C. F.; Dong, J. M. *Phys. Rev. B* **2005**, *72*, 205428. (b) Fa, W.; Dong, J. M. *J. Chem. Phys.* **2006**, *124*, 114310. (c) Tian, D. X.; Zhao, J. J. *J. Phys. Chem. A* **2008**, *112*, 3141.

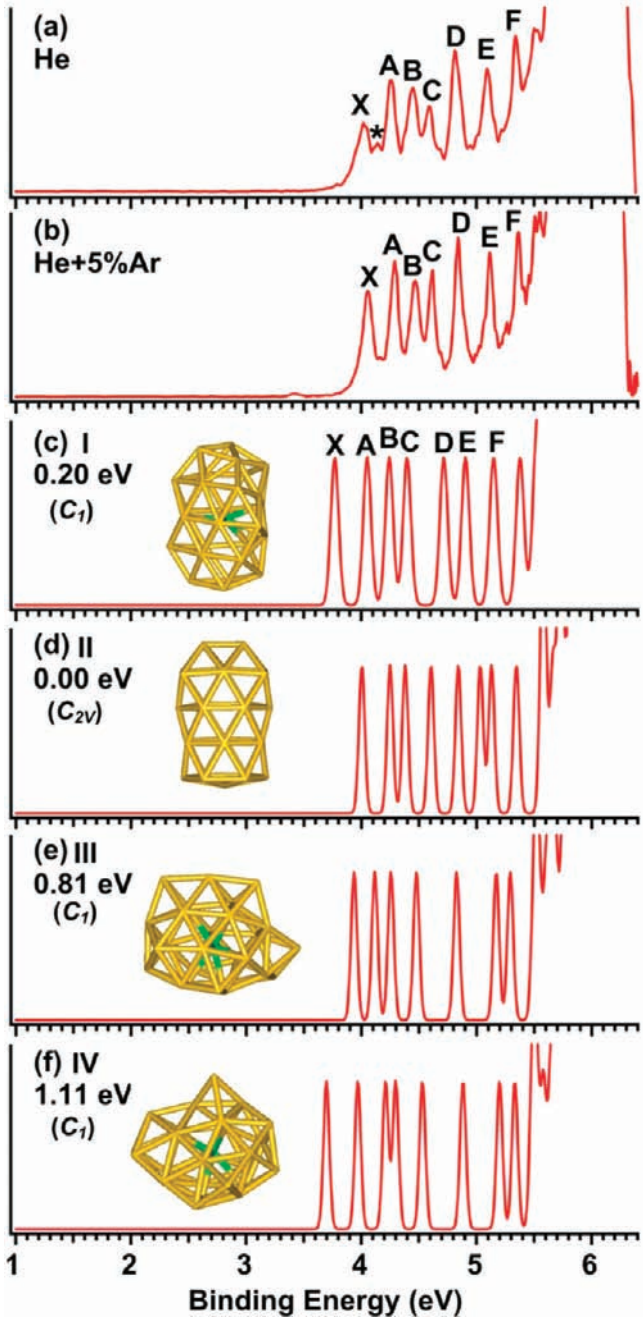

Figure 1. Photoelectron spectra of Au_{27}^- at 193 nm taken with (a) a pure He carrier gas and (b) a 5% Ar-seeded He carrier gas. (c) Simulated spectrum of one-atom core−shell isomer I. (d) Simulated spectrum of tubular isomer II.[28] (e, f) Simulated spectra of one-atom core−shell isomers III and IV.

result of the enhanced cooling by Ar seeding. In particular, the weak feature between X and A labeled as "*" in Figure 1a was no longer present in Figure 1b under the colder condition. Surprisingly, the * feature was significantly enhanced in the 266 nm spectrum (Figure S1) using the pure He carrier gas. These observations suggest that this weak feature most likely stems from a low-lying isomer. There are also obvious variations of relative intensities among the resolved peaks between the two spectra, probably as a result of the presence of the minor isomer in Figure 1a.

The simulated spectra of Au_{27}^- and the corresponding structures of four low-lying isomers (I−IV) are shown in Figure 1c−f. In terms of the overall spectral pattern (i.e., the relative peak spacings), the simulated spectrum of isomer I agrees best with the experimental spectra. The main features in the experimental spectra (X and A−F) are reproduced very well in the simulated spectrum (Figure 1c). Note that the simulated spectrum is red-shifted by ∼0.1−0.3 eV relative to the experimental spectra. We found previously that this is caused by the PBE0/CRENBL calculation with the inclusion of the SO effects.[17a] The energy of isomer I is 0.2 eV higher than that of the tubular isomer II[28] at the PBE0/CRENBL/SO level. We also calculated the energies of both isomers at the M06-L/CRENBL/SO level (implemented in NWChem 5.1.1) and found that isomer I is 0.75 eV lower in energy than isomer II. Two groups have recently shown that the M06-L functional gives a more accurate energy ranking for small gold anion clusters than the PBE0 functional does.[4d,e]

Table 1. Observed Vertical Detachment Energies (VDEs) for the First (X) and Second (A) PES Bands for Au_n^- (n = 27, 28, 30, and 32−35)[a]

	VDE (X)	VDE (A)	Δ[VDE(A) − VDE (X)]
Au_{27}^-	4.05	4.27	0.22
Au_{28}^-	3.86	4.08	0.22
Au_{30}^-	3.93	4.15	0.22
Au_{32}^-	4.03	4.34	0.31
Au_{33}^-	4.18	∼4.4	∼0.2
Au_{34}^{-}[b]	3.42	4.36	0.94
Au_{35}^-	4.11	4.42	0.31

[a] All energies are in eV. The uncertainty in all VDEs was ±0.03 eV. [b] From ref 13c.

The simulated spectral pattern of tubular isomer II (Figure 1d)[28] does not agree well with the experimental spectra and may be ruled out as the main isomer. However, the calculated electron binding energies of isomer II are slightly higher than those of isomer I, and the first peak of isomer II could correspond to the weak feature labeled * in Figure 1a. The other two low-lying isomers (III and IV in Figure 1) can be ruled out as the carriers of the main spectral features because they are much higher in energy and their simulated spectral patterns do not match well with the major PES features. These results indicate that the relative energies calculated from the PBE0 functional can carry errors of several tenths of an electronvolt. Hence, good agreement between theoretical and experimental PES spectra is a better criterion for the assessment of viable structures. It may not be reliable to assign global minimum structures solely on the basis of the DFT energy ranking. Comparison with experimental data along both PBE0 and M06-L energy ranking seems to be a better means of cluster structural assessment.

We examined a total of 21 low-lying isomers for Au_{27}^-, which give rise to energy gaps between the first and second PES peaks close to the experimental observation. Most of these low-lying isomers exhibit core−shell structures, such as isomers I, III, and IV. Isomer I possesses a relatively round cylindrical structure with one atom in the center, whereas isomers III and IV both possess highly irregular structures. The tubular isomer II with C_{2v} symmetry in Figure 1d was previously predicted to be the global minimum for neutral Au_{27}.[28c] Besides the good agreement between the simulated and measured PES spectra, the large population of low-lying core−shell structures for Au_{27}^- provides credence to our conclusion that the global minimum of Au_{27}^- is a core−shell structure with a one-atom core. However, the good agreement of the first peak from isomer II

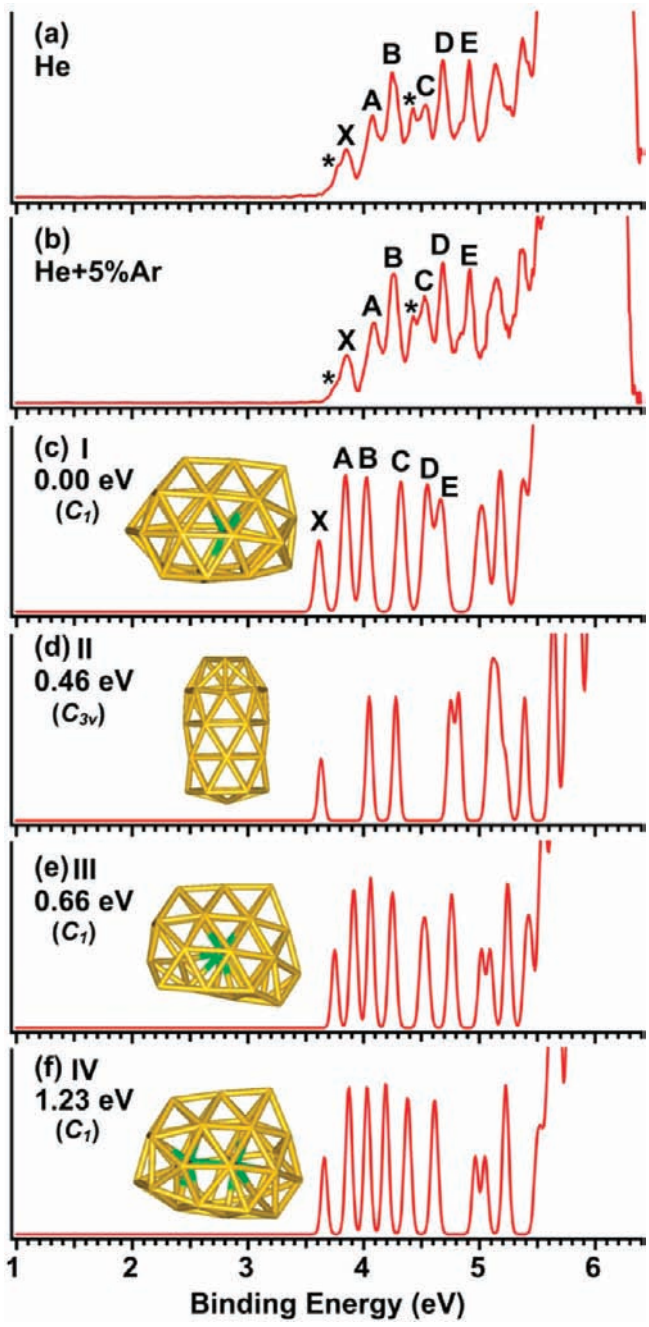

Figure 2. Photoelectron spectra of Au_{28}^- at 193 nm taken with (a) a pure He carrier gas and (b) a 5% Ar-seeded He carrier gas. (c) Simulated spectrum of core−shell isomer I. (d) Simulated spectrum of tubular isomer II.[28] (e) Simulated spectrum of one-atom core−shell isomer III. (f) Simulated spectrum of two-atom core−shell isomer IV.

(Figure 1d) with observed minor peak * in Figure 1a suggests that the tubular structure may be a viable low-lying isomer. The fact that the * peak is enhanced at 266 nm implies that isomers I and II are very close in energy. Finally, we note that the gold atoms on the shell of isomer I display a helical arrangement. Thus, the global minimum of Au_{27}^- is chiral, although all C_1 clusters are chiral.

Au_{28}^-. The 193 nm spectra of Au_{28}^- using the pure He carrier gas and Ar-seeded He carrier gas are shown in Figure 2a,b, respectively. There are no major differences between the two spectra, but some subtle variations are discernible. The main differences are the weak features labeled with *: their relative intensities are reduced in the Ar-seeding experiment. This observation suggests that these weak features likely originated from a minor low-lying isomer whose population was reduced in the cluster beam under the colder condition of the Ar-seeded carrier gas. A number of discrete peaks were resolved in the low-binding-energy range in the 193 nm spectra of Au_{28}^-, as labeled in Figure 2a,b. Peaks X and A define a HOMO−LUMO gap of 0.22 eV for neutral Au_{28} (Table 1).

In our global minimum search for Au_{28}^-, a total of 13 candidate isomers were considered, but only isomer I meets all three criteria mentioned above (Figure 1c). This isomer is the lowest in energy at the PEB0/CRENBL/SO level with a simulated spectrum in good agreement with the experimental data. This isomer consists of a core−shell structure with a one-atom core. The next isomer, II, which is 0.46 eV higher in energy, is a tubular structure with C_{3v} symmetry that was considered previously for neutral Au_{28}.[28c] This isomer is built upon isomer II of Au_{27}^- (Figure 1d). The simulated spectrum of this isomer is totally different from the main features of the experimental data. However, this isomer may be the carrier for the weak isomer with the first two features corresponding to the experimental features labeled as * (Figure 1b). Isomers III and IV are core−shell structures with one and two core atoms, respectively, but their relative energies become significantly higher with the inclusion of the SO effects and thus are not competitive for the global minimum of Au_{28}^-. Thus, the Au_{28}^- cluster is similar to Au_{27}^-, with each consisting of a core−shell global minimum with a single core atom and a tubular low-lying isomer.

Au_{30}^-. The 193 nm spectra of Au_{30}^- are remarkably simple with only six well-resolved bands in the low-binding-energy region (Figure 3a,b). The spectra with the pure He carrier gas (Figure 3a) or Ar-seed He carrier gas (Figure 3b) are identical, suggesting that there is only one isomer in the Au_{30}^- beam. The relative intensity of the fourth band is higher with a broader bandwidth, indicating that there may be two unresolved features (C and D) beneath this band that are indeed resolved in the 266 nm spectrum (Figure S1). The X and A bands define a HOMO−LUMO gap of 0.22 eV for neutral Au_{30} (Table 1).

Our global-minimum search for Au_{30}^- yielded a total of 21 candidate isomers that meet criteria 1 and 2 above, and their PES spectra were computed. Among the 21 candidate isomers, 14 contain a 2-atom core, 5 contain a 1-atom core, and 2 contain a 3-atom core. However, only three isomers give simulated spectra that display some resemblance to the experimental data, as shown in Figure 3c−e. Among the three, the simulated spectrum of isomer I is in quantitative agreement with the experimental data in terms of the overall spectral pattern, peak positions, and spacings, leaving little doubt that isomer I is the global minimum for Au_{30}^-. Isomers II and III can be readily ruled out because their detailed spectral spacings are inconsistent with the experimental data. Even though isomer I is 0.17 eV higher in energy than isomer II, this is well within the error of the PBE0 functional, as shown above for Au_{27}^-. The fact that there is no experimental hint of the presence of low-lying isomers suggests that the true energy of isomer II should be much higher.

The global minimum isomer I of Au_{30}^- consists of a 1-atom core and a 29-atom shell, whereas both isomers II and III contain a 2-atom core. Therefore, the current results suggest that the two-atom core structures are still not competitive for Au_{30}^- and that the Au_n^- clusters grow by expanding the shell from Au_{27}^- to Au_{30}^-.

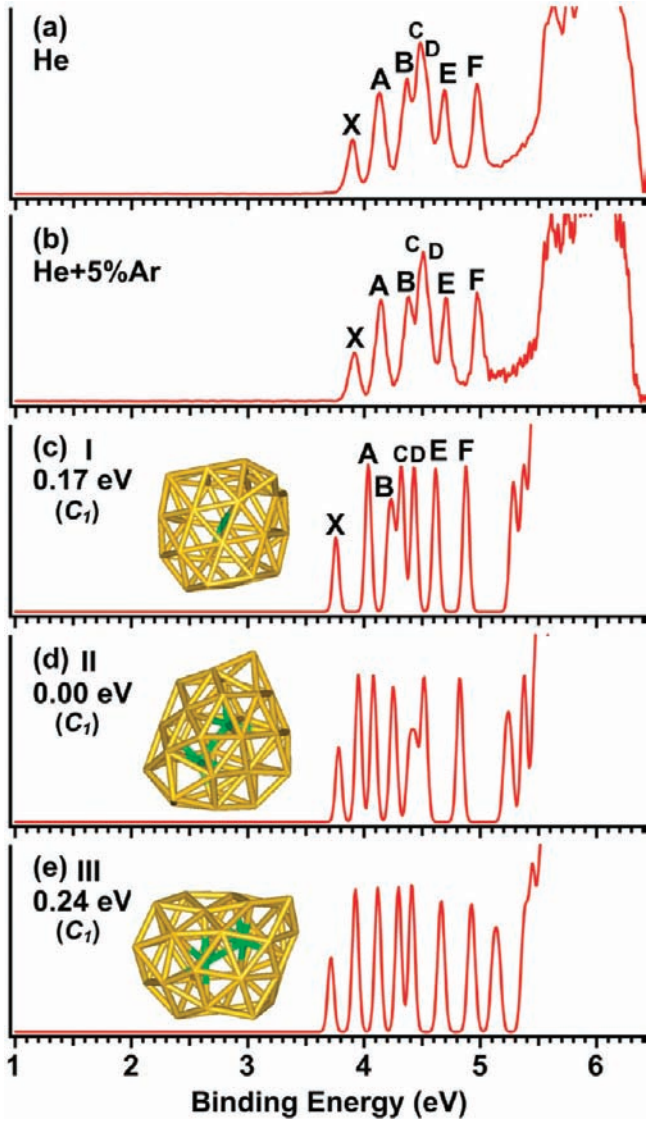

Figure 3. Photoelectron spectra of Au_{30}^- at 193 nm taken with (a) a pure He carrier gas and (b) a 5% Ar-seeded He carrier gas. (c) Simulated spectrum of one-atom core−shell isomer I. (d, e) Simulated spectra of two-atom core−shell isomers II and III.

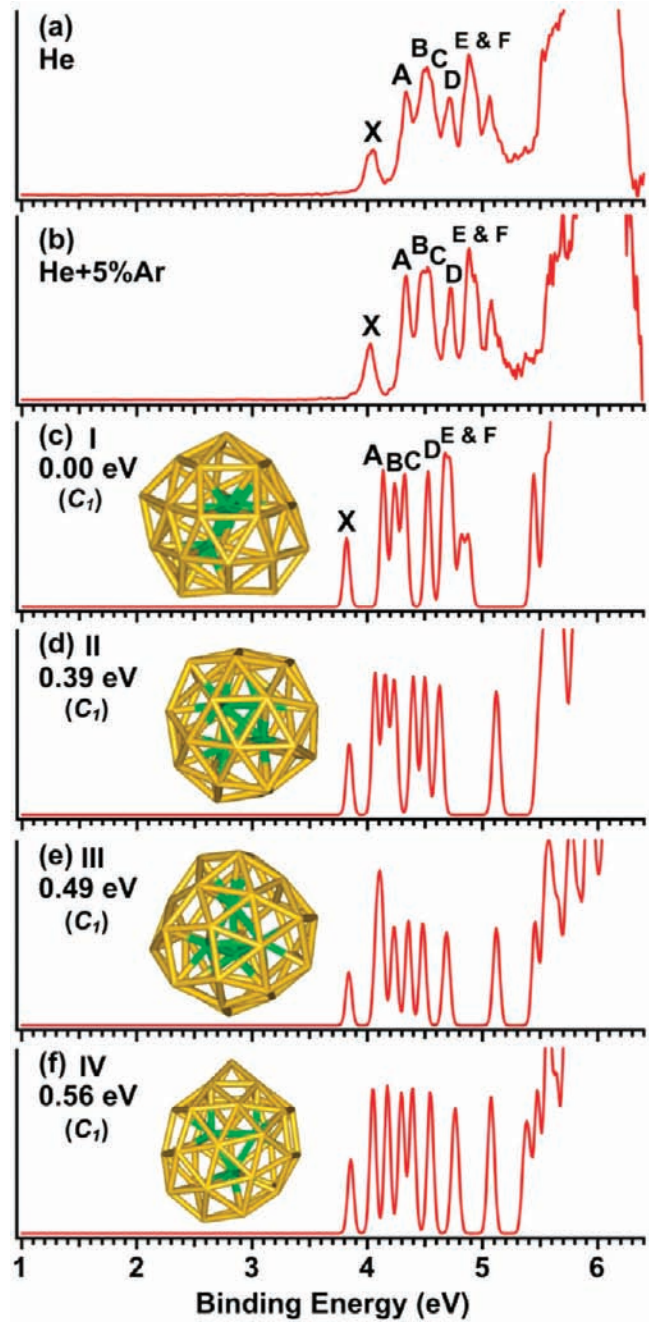

Figure 4. Photoelectron spectra of Au_{32}^- at 193 nm taken with (a) a pure He carrier gas and (b) a 5% Ar-seeded He carrier gas. (c) Simulated spectra of the best three-atom core−shell isomer, I. (d−f) Simulated spectra of three previously reported best candidate isomers II,[12b] III,[12c] and IV.[12a]

Au_{32}^-. Neutral Au_{32} has been predicted to be a fullerene-like hollow cage structure with icosahedral (I_h) symmetry and a large HOMO−LUMO gap (0.8 eV) using DFT calculations.[14] A subsequent joint PES and theoretical study showed that the cage structure for the Au_{32}^- anion is not the most stable structure.[12a] Instead, the most likely structure for Au_{32}^- consists of a low-symmetry core−shell structure with a three-atom core. The prediction of low-symmetry core−shell structure was confirmed by further DFT calculations by Garzon and co-workers[12b] and Johansson et al.[12c] Both groups suggested that a core−shell structure with a four-atom core may be the global minimum. To resolve this discrepancy, we carried out further studies on Au_{32}^-. We measured the PES of Au_{32}^- again at 193 nm using the Ar-seeded He carrier and found that the spectrum (Figure 4b) was slightly better resolved than the previous measurement using a pure He carrier gas (Figure 4a).[12a] The relative intensities of the resolved peaks in the low-binding-energy range remain similar under the two experimental conditions, suggesting that there was only one dominating isomer in the Au_{32}^- beam.

We carried out BH global minimum searches for Au_{32}^-. A total of 11 candidate isomers were found to meet criteria 1 and 2 mentioned above, and nearly all of these candidate isomers are of the core−shell type with a three-atom triangular core, consistent with the previous PES and DFT study.[12a] Among the 11 candidate isomers, we found that the simulated spectrum of the lowest-energy structure I (Figure 4c) agrees best with the experimental spectrum. The resolved features from X to F (Figure 4b) in the low-binding-energy region and the following energy gap are all well reproduced by the simulated spectrum, providing considerable credence for isomer I as the global minimum of Au_{32}^-. We

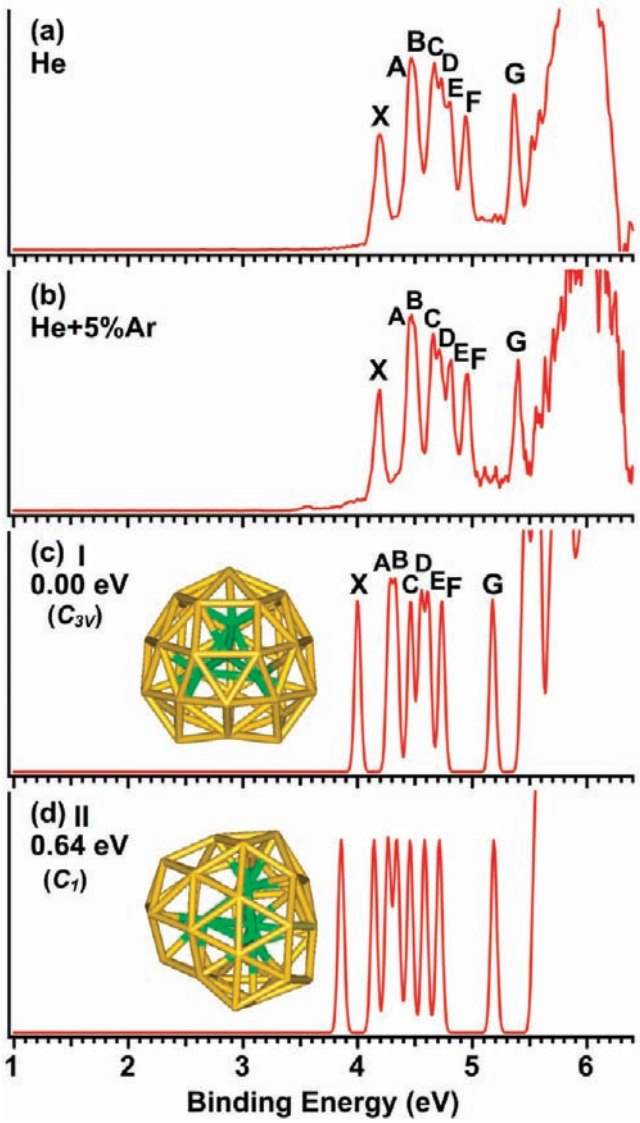

Figure 5. Photoelectron spectra of Au_{33}^- at 193 nm taken with (a) a pure He carrier gas and (b) a 5% Ar-seeded He carrier gas. (c, d) Simulated spectra of four-atom core−shell isomers I and II.

will show below that the outer layer of isomer I is actually a common shell motif for the growth of gold clusters from Au_{33}^- to Au_{35}^-.

For comparison, we recalculated the core−shell structures reported previously for Au_{32}^-: two with a four-atom core (Figure 4d,e)[12b,c] and one with a three-atom core (Figure 4f).[12a] We found that all of these structures are higher in energy than isomer I identified in the current study. The simulated spectra of structures II and IV display some resemblance to the experimental spectra, but the agreement is clearly inferior relative to that of isomer I. Specifically, the peak just above 5 eV in the simulated spectra does not agree with the experimental data, which display a large gap between the well-resolved low-binding-energy features (<5 eV) and the congested high-binding-energy features (>5.5 eV).

Au_{33}^-. For Au_{33}^-, the 193 nm spectra using the pure He carrier gas (Figure 5a) and the Ar-seeded He carrier gas (Figure 5b) also display no significant difference, except that peak E in Figure 5b is slightly better resolved. The spectra of Au_{33}^- are relatively simple. The second band appears to contain unresolved components (A and B), which are better resolved in the 266 nm spectrum (Figure S1): the A band appears as a shoulder, making it difficult to estimate its VDE. Features C−E are also rather congested and closely spaced. The relative intensities of the main features remain the same under the two experimental conditions, suggesting that there is one dominating isomer in the Au_{33}^- beam.

Among more than 250 isomers generated in our BH searches, only 5 isomers meet the criteria 1 and 2 above. Many isomers of Au_{33}^- can be easily ruled out on the grounds that the energy gap between the first and second peaks is typically <0.1 eV, which is much less than the experimental observation (~0.2 eV, Table 1). Among the five candidate isomers, four contain a four-atom tetrahedral core and one contains a three-atom triangular core similar to isomer I of Au_{32}^-. The simulated spectrum of the lowest-energy isomer, I, (Figure 5c) agrees very well with the experimental spectra. In particular, the overlapping A and B features and the congested C−E features are well reproduced in the simulated spectrum. Low-lying isomer II is 0.64 eV above the global minimum (at the PEB0/CRENBL/SO level), and its simulated spectrum does not agree with the experiment as well as that of isomer I. It is noteworthy that the isolated peak above 5 eV (G) seems to be characteristic of the four-atom core. The simulated spectra of all isomers with a four-atom core, including those of Au_{32}^- (Figure 4d,e) give rise to a similar feature. This feature is in excellent agreement with the experimental observation, confirming that the three-atom to four-atom core transition occurs from Au_{32}^- to Au_{33}^-.

Au_{34}^-. Neutral Au_{34} represents a major shell closing. Indeed, the PES spectra of Au_{34}^- display a large HOMO−LUMO energy gap.[11] This observation has stimulated major previous efforts to elucidate the structures of Au_{34}^- by the Kappes group using a combination of TIED/PES and DFT calculations[13a] and by our group using a combination of PES and DFT calculations.[13c] Both groups concluded that the global minimum of Au_{34}^- consists of a core−shell structure with a four-atom tetrahedral core, but there are some notable structural differences in the details of the outer layer (shell). Kappes and co-workers reported a global minimum structure for Au_{34}^- with C_3 symmetry,[13a] originally proposed by Doye and Wales,[13b] whereas Gu et al. reported that two low-symmetry C_1 structures compete for the global minimum for Au_{34}^-.[13c] To resolve this discrepancy, we have carried out further studies. Experimentally, we remeasured the 193 nm spectrum of Au_{34}^- using the Ar-seeded He carrier gas, but the spectrum is identical to that previously measured using the pure He carrier gas, as shown in Figure 6a. The large X−A gap corresponds to the large HOMO−LUMO gap in neutral Au_{34}, followed by a set of well-resolved peaks (A−H) in the low-binding-energy range.

A database of low-lying isomers is already available for Au_{34}^- from the previous studies,[13c] although the SO effects were not considered in the previous calculations of the PES spectra for Au_{34}^-. In the current study, we reoptimized more than 280 isomers obtained from the database at a higher level of theory (the fine level in DMol3). Fifteen isomers meet criteria 1 and 2 above, and they all exhibit the core−shell-type structure with a four-atom tetrahedral core, confirming that the four-atom core is very robust in this size range.

In our previous study, the two C_1 structures (named 34a and 34b) and the C_3 structure (named 34c) were the lowest-

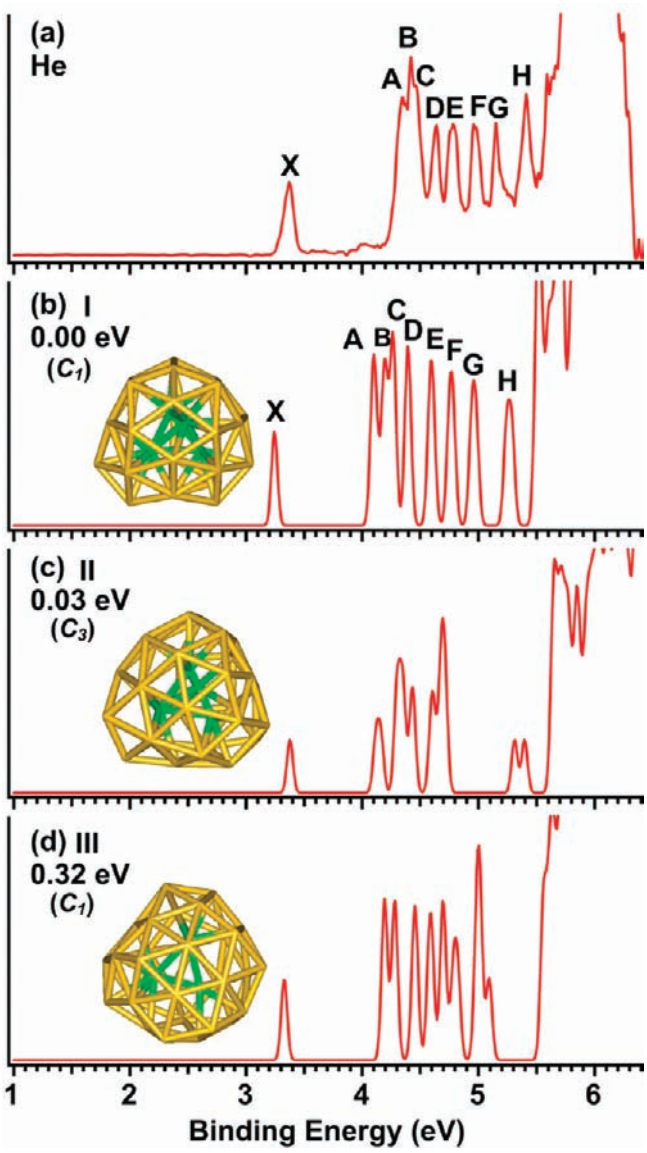

Figure 6. (a) Photoelectron spectrum of Au_{34}^- at 193 nm. (b) Simulated spectrum of the best candidate isomer, four-atom core−shell isomer I (ref 13c, isomer b). (c, d) Simulated spectra of two previously reported best candidate isomers, II (ref 13a isomer 1, or ref 13c, isomer c) and III (ref 13c, isomer a).

lying isomers within 0.1 eV using the PBE functional.[13c] In the current work using PBE0/CRENBL/SO, these three structures remain the lowest-lying isomers, as shown in Figure 6b−d and labeled as isomers I−III, respectively. Isomer I corresponds to 34b in our previous study, which is nearly degenerate with isomer II (C_3 structure 34c) in the current study. Previous isomer 34a (isomer III, Figure 6d), which was nearly degenerate with 34b, becomes 0.32 eV higher in energy than isomer I (i.e., previous isomer 34b) at the PBE0/CRENBL/SO level. Without the inclusion of the SO effects, our previous simulated PES spectra for both 34a and 34b were similar and both were in reasonable agreement with the experimental spectra and could not be distinguished. However, with the inclusion of the SO effects, the simulated spectra of isomer I (34b) and isomer III (34a) are very different in the binding-energy region between 4 and 5.5 eV and only that of isomer I agrees well with the experiment. Our previous simulated PES spectrum for the C_3 isomer (34c)

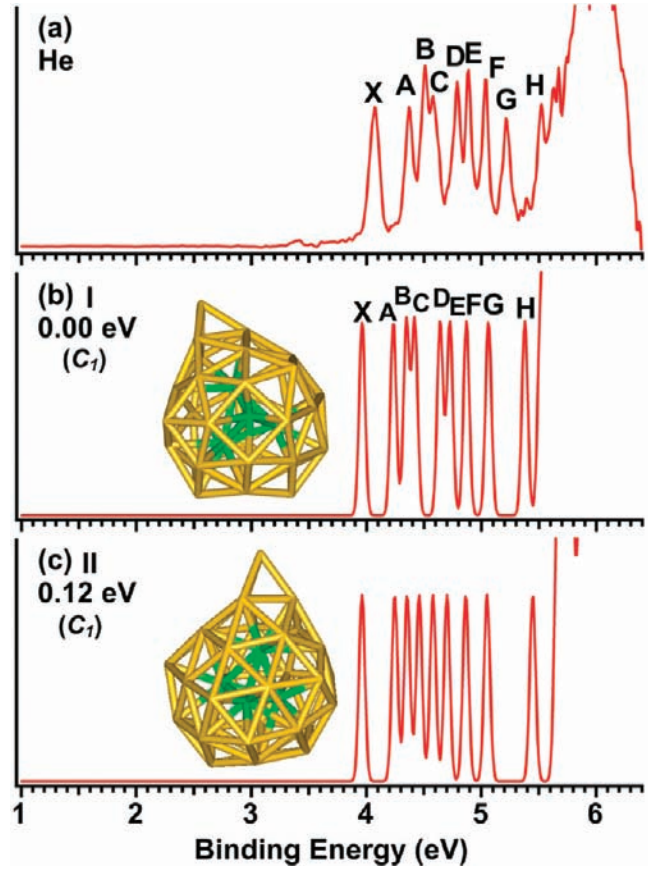

Figure 7. (a) Photoelectron spectrum of Au_{35}^- at 193 nm. (b, c) Simulated spectra of four-atom core−shell candidate isomer I and II.

did not agree with the experimental data. With the inclusion of the SO effects, the simulated spectrum of the C_3 isomer is still found to disagree with the experiment, as can be seen clearly in Figure 6c. The excellent agreement between the simulated spectrum of isomer I (Figure 6b) and the experimental data confirms that the global minimum of Au_{34}^- should be the low-symmetry C_1 structure with a four-atom tetrahedral core. This conclusion is also supported by two recent studies[13d,e] that showed that the Au_{34}^- cluster favors a low-symmetry structure with a four-atom tetrahedral core.

Au_{35}^-. The 193 nm spectrum of Au_{35}^- is shown in Figure 7a. Similar to Au_{34}^-, the spectra taken using either the pure He carrier gas or the Ar-seeded He carrier gas are virtually identical, suggesting that the Au_{35}^- beam is dominated by one major isomer. Nine well-resolved peaks are observed in the PES spectrum in the low-binding-energy range. In fact, the features from A to H are somewhat similar to the corresponding bands in the spectrum of Au_{34}^- (Figure 6a). Au_{34}^- is open-shell with a single electron occupying the LUMO of the neutral cluster, giving rise to the X band in the PES spectrum. The PES spectrum of Au_{35}^- suggests that it is closed-shell as judged by the high relative intensity of the X band (Figure 7a). One can see that the extra electron in Au_{35}^- pairs up with the single electron in Au_{34}^-, suggesting that they may have similar atomic structures.

Our theoretical calculations revealed a total of nine candidate isomers for Au_{35}^- that meet criteria 1 and 2, and all of these candidate isomers exhibit core−shell structures with a four-atom tetrahedral core. The simulated spectra of

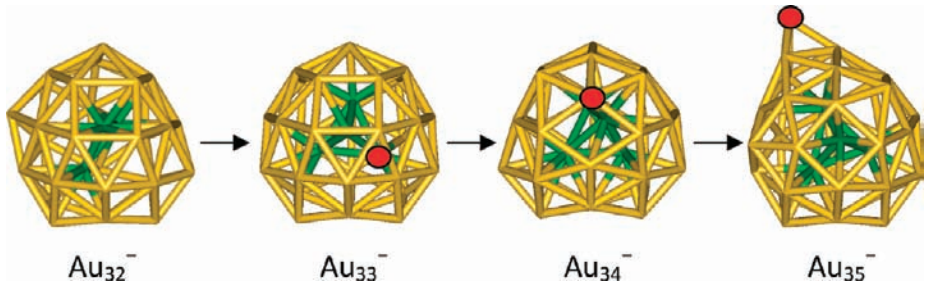

Figure 8. Growth pattern from Au_{32}^- to Au_{35}^-. Newly added atoms are highlighted in red.

the two lowest-energy isomers are compared with the experimental data in Figure 7. These two isomers can both be viewed as adding the extra Au atom to the surface of the Au_{34}^- cluster. The overall spectral pattern from the lowest-energy isomer, I, (Figure 7b) is in excellent agreement with the experimental spectrum, providing strong evidence for the identified global minimum of Au_{35}^-. Global minimum isomer I of Au_{35}^- is similar to that of Au_{34}^- by adding the extra atom to the surface, consistent with their similar PES spectral features.

Structural Evolution and Growth Pattern of Midsized Gold Clusters. Although Au_{32} has been suggested to be an icosahedral cage, the Au_{32}^- anion is definitely shown to be a low-symmetry core−shell structure with a three-atom core. Tubular-type low-symmetry structures without an internal atom have been shown to be low-lying isomers for Au_{27}^- and Au_{28}^-, but their global minimum structures appear to be core−shell structures with a single-atom core. Previously, we showed that the onset of core−shell structures was at Au_{25}^-, which features a single-atom core. Structures with a two-atom core were only found to be low-lying isomers computationally for Au_{30}^-, but its global minimum was confirmed to contain only a single-atom core by the excellent agreement between the simulated and experimental PES spectra (Figure 3). No clusters were found to contain a two-atom core because the next cluster that we studied was Au_{32}^-, which contains a three-atom core. The Au_{31}^- cluster, which is omitted in the current study, is mostly likely to contain a two-atom core. It is conceivable that the two-atom core is not structurally sound such that other structural types are competing for the global minimum, thus resulting in the congested PES spectra for Au_{31}^- (Figures S1 and S2). The three-atom core is also proven to be unpopular because the global minimum of Au_{33}^- is firmly shown to contain a four-atom core. The four-atom tetrahedral core seems to be rather robust, and it is present in both Au_{34}^- and Au_{35}^- and possibly in even larger clusters.

When the global minimum structures of Au_{32}^- to Au_{35}^- are compared (Figure 8), an interesting structural evolution can be recognized. Besides their common four-atom tetrahedral core, the lowest-energy structures of Au_{33}^- to Au_{35}^- all have a similar outer layer, which is the shell of the global minimum of Au_{32}^-. The structures from Au_{33}^- to Au_{35}^- can be viewed on the basis of the structure of Au_{32}^-. As shown schematically in Figure 8, Au_{33}^- can be viewed as adding one Au atom to the core of Au_{32}^-. Hence, Au_{32}^- and Au_{33}^- have the same outer layer with relatively minor structural relaxations: the shell of Au_{33}^- is more round in shape because of the more symmetric tetrahedral core. However, the larger size of the tetrahedral core appears to cause a significant strain on the shell of Au_{33}^-, resulting in six rhombus "defects", whereas the shell of Au_{32}^- contains only one rhombus "defects". The next Au atom goes into the center of a rhombus defect site on the surface of the Au_{33}^- cluster to form Au_{34}^-, expanding the outer layer to a 30-atom shell. After structural relaxation, the 30-atom outer layer of Au_{34}^- exhibits only three rhombus defects. Interestingly, the next Au atom does not go into a similar rhombus site on Au_{34}^- to form Au_{35}^-. Rather, Au_{35}^- can be viewed as adding one Au atom to the shell of Au_{34}^- by starting a new layer. The structure of Au_{35}^- is a manifestation of the stability of the closed-shell Au_{34} cluster. We have observed previously a similar growth pattern from the closed-shell, highly stable Au_{58}^- cluster.[16] Additional atoms from Au_{59}^- to Au_{65}^- were found to nucleate on the surface of the highly stable, spherical Au_{58}^- cluster to form a new layer without significantly altering its structure. Thus, it is expected that clusters larger than Au_{35}^- may continue to grow by nucleating onto the surface of Au_{34}^-. Then, at a certain critical size, a major structural transition may occur.

Conclusions

We have carried out a joint experimental and theoretical investigation to elucidate the structural evolution of Au_n^- clusters in the size range of $n = 27-35$. Well-resolved photoelectron spectra were obtained using an Ar-seeded He carrier gas for better cluster cooling. For Au_{27}^- and Au_{28}^-, both experimental and computational evidence indicates that minor tubular-type isomers contributed to the experimental spectra, confirming the viability of such hollow structures as low-lying isomers. We found that the most stable structures of the midsized gold clusters, Au_n^- ($n = 27$, 28, 30, and 32−35), all exhibit core−shell type structures with different core atoms: Au_{27}^-, Au_{28}^- and Au_{30}^- all contain a one-atom core, Au_{32}^- contains a three-atom triangular core, and Au_{33}^- to Au_{35}^- all feature a four-atom tetrahedral core. A cluster growth path was identified from Au_{27}^- to Au_{35}^-: from Au_{27}^- to Au_{30}^- the clusters, which all have a single-atom core, grow by expanding the shell ($Au@Au_m^-$, $m = 26-29$); Au_{33}^- ($Au_4@Au_{29}$) can be viewed as adding an Au atom to the core of Au_{32}^- ($Au_3@Au_{29}$) whereas Au_{34}^- ($Au_4@Au_{30}$) can be viewed as adding an Au atom to the shell of Au_{33}^- ($Au_4@Au_{29}$). The Au_{34}^- structure, featuring a tetrahedral core and a 30-atom shell, is observed to be more round and quite robust, and the Au_{35}^- cluster can be viewed as adding an Au atom onto the surface of Au_{34}^-: [($Au_4@Au_{30}$) + Au]. The observed core−shell growth path is interesting and may provide a valuable guide to the search for structures of larger gold clusters.

Acknowledgment. We thank Professor Xingao Gong for valuable discussions. The experimental work was supported by

the National Science Foundation (CHE-0749496). NWChem calculations were performed using the supercomputer at the EMSL Molecular Science Computing Facility of the Pacific Northwest National Laboratory. W.H. thanks Dr. Niranjan Govind for invaluable assistance with the spin−orbit calculations using NWChem. The theoretical work done at Nebraska was supported by grants from the National Science Foundation (DMR-0820521), the Nebraska Research Initiative, and the University of Nebraska Holland Computing Center.

Supporting Information Available: Photoelectron spectra of Au_n^- ($n = 27-35$) at 266 nm and those of Au_{29}^- and Au_{31}^- at 193 nm, relative energies and energy gaps for candidate low-lying isomers for $n = 27$, 28, 30, and 32−35, and the complete citation of ref 26. This material is available free of charge via the Internet at http://pubs.acs.org.

JA102145G